Separation of Protein Charge Variants with Induced pH Gradients Using Anion Exchange Chromatographic Columns

Timothy M. Pabst* and Giorgio Carta
Dept. of Chemical Engineering, University of Virginia, 102 Engineers' Way, Charlottesville, VA 22904-4741

Natrajan Ramasubramanyan, Alan K. Hunter, Paul Mensah, and Mark E. Gustafson
Pfizer, Inc., Global Biologies, 700 Chesterfield Parkway West, Chesterfield, MO 63017

DOI 10.1021/bp.53
Published online September 26, 2008 in Wiley InterScience (www.interscience.wiley.com).

This work concerns the chromatographic separation of protein charge variants using pH gradients generated by step changes in buffer composition with weak base anion exchange columns. A local equilibrium model is first developed to describe pH transitions occurring in the column using buffers comprising neutral, zwitterionic or positively charged species. Model predictions, based solely on the resins' titration curves and obtained with the method of characteristics, show, in excellent agreement with experiments, that induced pH gradients of varying durations and shapes can be obtained with a broad range of buffer systems including Tris, Bis-Tris propane, histidine, and their mixtures and ethanolamine. The separation of protein charge variants is then demonstrated for bovine apo-transferrin and for a monoclonal antibody. The resolution of the charge variants present in these proteins, demonstrated via isoelectric focusing analyses, is obtained for conditions amenable to scale-up for preparative purposes; that is larger particle sizes (90 μm), higher flow rates (100–600 cm/h), and higher protein loads (2–5 mg/mL). Because the approach requires only step changes in buffer composition and commonly available, unretained buffers species, practical implementation is straightforward. The focusing effect of the induced pH gradient results in relatively sharp peaks and substantial resolution even for these conditions.
Keywords: pH gradient elution, protein chromatography, ion exchange, local equilibrium theory, protein charge variants

Introduction

The separation of protein charge variants is an important endeavor in a number of biotechnology applications. Such variants occur during expression as a result of posttranslational modifications or arise in manufacturing as a result of chemical or enzymatic actions.[1–4] A number of authors have shown that charge variants of therapeutic proteins can have vastly different bioactivity. For example, Yem et al.[5] showed that N-terminal analogues of recombinant human interleukin-1β (IL-1β) were threefold to sixfold less active than the native protein. Similarly, Harris et al.[6] showed that deamidated variants of recombinant human monoclonal antibodies had reduced potency in a bioactivity assay. Other authors[7–11] have shown that differences in sialic acid content lead to varying cellular cytotoxicity and pharmacokinetics for various proteins.

Although upstream modifications can some times be used to reduce or eliminate charge variants[12,13] downstream processing is often used to separate them. For example, ion exchange chromatography with salt gradients has been used to separate N-terminus variants of recombinant IL-1β,[5] C-terminus variants of monoclonal antibodies (mAbs),[14] deamidated variants of mAbs[6] and ribonuclease A,[14] amino acid variants of β-lactoglobulin,[15] and sialylated variants of human serum transferrin.[16] In general, however, a disadvantage of salt gradient elution is the need for gradient mixing, which can be cumbersome to implement on a process scale. Moreover the protein is eluted in high salt, which, in turn, may have to be removed before the next processing or formulation step.

An alternative to salt gradient elution is elution with pH gradients. In this approach, ideally the charge variants are eluted in order of their pI, with more acidic proteins eluting earlier in cation exchangers and later in anion exchangers in a manner analogous to isoelectric focusing (IEF). pH gradients can be implemented in different ways. One approach is to use strong exchangers with externally generated temporal pH gradients formed by mixing mobile phases containing nonretained buffering species prepared at high and low pH values. For example, separations of isoforms with pH gradients have been shown for deamidated variants of a mAb[17] and of recombinant interleukin,[18] for amino acid variants of β-lactoglobulin,[19] and for phosphorylated variants of ovalbumin.[20] Much like salt gradients, externally generated temporal pH

*Current address of T. M. Pabst: Pfizer, Inc., Global Biologies, 700 Chesterfield Parkway West, Chesterfield, MO 63017

Correspondence concerning this article should be addressed to G. Carta at gc@virginia.edu.

gradients are sometimes difficult to implement in large scale due to the mixing requirements. Moreover, proteins applied to the column under strong binding conditions merely sit at the column entrance until the pH is sufficiently low so that elution occurs.

Another approach is to generate pH gradients internally using strong ion exchangers with a step in mobile phase composition using buffer species that are adsorbed on the stationary phase. This process, known as chromatofocusing, is typically implemented with complex mixtures of zwitterionic buffers known as "ampholytes."[21,22] The result is an axial pH gradient that moves down the column. The separation of charge variants starts instantly as these species become focused along pH waves where the chromatographic velocity of the protein equals the velocity of the pH wave, in a manner similar to IEF. The existence of a substantial axial pH gradient in chromatofocusing system is thought to be the reason for the higher resolution obtained is compared to externally generated temporal pH gradients. However, as discussed by Strong and Frey,[23] chromatofocusing buffers are expensive and tend to associate with proteins.[24] On the other hand, more recent work has shown that internal pH gradients can also be generated using nonadsorbed buffers or their mixtures using weak cation or anion exchangers.[25–29] Because in these cases the buffer species are not adsorbed, they do not compete for ion exchange sites nor do they usually associate with proteins.

In this article we explore the generation of induced pH gradients with two commercial weak anion exchangers, DEAE Sepharose FF and ANX Sepharose FF, using step changes in buffer composition and their use for the separation of protein charge variants. A local equilibrium model, based on the resins' titration curves, is developed and used to successfully predict the shape and duration of the gradients induced by different buffer combinations. Two different examples of protein charge variant separations are then considered. The first is the separation of bovine apotransferrin charge variants whereas the second is the separation of monoclonal antibody charge variants. In both cases, unlike most prior work, the resolution of charge variants, demonstrated by analytical IEF, is obtained using large diameter stationary phases (90 μm), higher protein loads (up to 5 mg/mL), and higher flow rates (up to 600 cm/h) than previously used.

Theoretical Development

The model used to predict the induced pH gradients is based on the framework of Bates and Frey[30] and parallels the development of Pabst et al.[31] for weak cation exchangers. We consider simultaneously solution and ion exchange equilibria and solve the column conservation equations by the method of characteristics. Because this work is largely an adaptation of our prior development for weak cation exchangers, only an abbreviated version of the theoretical development is presented.

Solution equilibria

Tris(hydroxymethyl)aminomethane (TRIS), 1,3-bis[tris(hydroxymethyl)methylamino] propane (BTP), and histidine (HIS) buffers and their mixtures are considered for the separation of apo-transferrin variants, which are known to have isoelectric points around 6.[32] TRIS is monoprotic with $pK_a = 8.06$, BTP is diprotic with $pK_a = 6.80$ and 9.00, and HIS is triprotic, with $pK_a = 1.70$, 6.04, and 9.28. All pK_as given are at 298 K and infinite dilution are from Refs. 33 and 34. The pH gradients generated with these buffers were typically between 5 and 7. For these conditions, only the monovalent cationic and the zwitterionic forms of HIS, corresponding to the second pK_a, are relevant. Ethanolamine with $pK_a = 9.52$ was used for the separation of antibody charge variants at pH values between 9.5 and 8. Its dissociation behavior is analogous to TRIS.

Considering a mixture of TRIS, BTP, and HIS, at each pH, the charged species must satisfy the electroneutrality condition:

$$C_{Cl^-} + C_{OH^-} = C_{TRIS^+} + C_{HIS^+} + C_{BTP^+} + 2C_{BTP^{2+}} + C_{H^+} \tag{1}$$

Coupling this equation with the expressions for the dissociation equilibrium of each buffering species, we obtain:

$$C_{Cl^-} + \frac{K_w}{C_{H^+}} = \frac{C_{TRIS}}{1 + \frac{K^1_{aT}}{C_{H^+}}} + \frac{C_{HIS}}{1 + \frac{K^2_{aH}}{C_{H^+}}} + \frac{C_{BTP}\left(K^1_{aB}/C_{H^+} + 2\right)}{1 + \frac{K^1_{aB}}{C_{H^+}} + \frac{K^2_{aB}}{C^2_{H^+}}} + C_{H^+} \tag{2}$$

where K_w is the ionic product of water and C_{TRIS}, C_{HIS}, and C_{BTP} are the total TRIS, HIS, and BTP concentrations, respectively. Note that activity coefficients are required to calculate corrected dissociation constants from the corresponding infinite dilution values accounting for the finite ionic strength of the solutions used. These corrections were made using the Davies equation[35] as described in Refs. 29 and 31. Given chloride and total buffer concentrations, Eq. 2 can be solved for C_{H^+} using Newton's method. The pH can then be calculated as $-\log_{10}(\gamma_{H^+}C_{H^+})$, where γ_{H^+} is from Eq. 10 in Ref. 31.

Ion exchange equilibria

In principle, the two resins considered in this work contain a single type of weak base group. Thus, ideally, a single *pK*-value should be sufficient to describe the resin's dissociation. In practice, however, a description with a single *pK*-value sometimes fails to represent the experimental behavior. This can occur because of chemical heterogeneity as well as because of interactions among neighboring functional groups. Accordingly, following Stoyanov and Righetti,[36] we represent the resin as a polyelectrolyte capable of n successive dissociations, each characterized by a dissociation constant

$$K_j = \frac{q_{R^{(j-1)+}}q_{H^+}}{q_{R^{j+}}}, \quad j = 1, 2 \ldots n \tag{3}$$

where all the q are resin phase concentrations. The resin phase electroneutrality condition is:

$$q_{Cl^-} + q_{OH^-} = \sum_{i=1}^{n} i q_{R^{i+}} + q_{H^+} \tag{4}$$

In practice, following Helfferich,[37] it can be seen that both q_{OH^-} and q_{H^+} are usually negligible. Thus, as an excellent approximation, we obtain:

$$q_{Cl^-} = \frac{q_0}{n} \frac{\sum_{i=1}^{n} \frac{i q_{H^+}^i}{\prod_{j=1}^{i} K_j}}{\left[1 + \sum_{j=1}^{n} \frac{q_{H^+}^j}{\prod_{k=1}^{j} K_k}\right]} \tag{5}$$

where q_0 is the total concentration of weak base groups. Lastly, on the basis of Donnan equilibrium,[37] we have:

$$q_{H^+} = \frac{C_{Cl^-} C_{H^+}}{q_{Cl^-}} \tag{6}$$

For given values of C_{Cl^-} and C_{H^+}, Eqs. 5 and 6 can be used to compute q_{Cl^-} using experimentally determined values of q_0, n, and K_j. The latter can be determined by fitting the model to data from a potentiometric resin titration experiment.

Column dynamics

The behavior of a column subject to step changes in buffer composition is determined by combining the solution and ion exchange equilibrium relationships described earlier with material balances for the column. The approach is illustrated here for the case of a TRIS/BTP/HIS buffer mixture. Mole balances are given by the equation:

$$\varepsilon \frac{\partial C_i}{\partial t} + (1 - \varepsilon) \frac{\partial \overline{q}_i}{\partial t} + \varepsilon v \frac{\partial C_i}{\partial z} = 0 \tag{7}$$

with $i = Cl^-$, TRIS, HIS, BTP and $\overline{q}_i = \varepsilon_p C_i + (1 - \varepsilon_p) q_i$. This equation assumes plug flow and neglects axial dispersion. The resulting system is solvable using the method of characteristics assuming local equilibrium with the further assumption that only Cl^- is bound to the resin. As a consequence $\overline{q}_i = \varepsilon_p C_i$ for each of the neutral, zwitterionic, and cationic buffering species. With this simplification, all buffering species have characteristic velocity:

$$v_{ci} = \frac{1}{1 + \phi \varepsilon_p} \tag{8}$$

Chloride, on the other hand, has characteristic velocities

$$v_{c_{Cl^-}} = \frac{v}{1 + \phi \left[\varepsilon_p + \left(1 - \varepsilon_p\right) \frac{dq_{Cl^-}}{dC_{Cl^-}}\right]} \tag{9}$$

and

$$v_{s_{Cl^-}} = \frac{v}{1 + \phi \left[\varepsilon_p + \left(1 - \varepsilon_p\right) \frac{q'_{Cl^-} - q''_{Cl^-}}{C'_{Cl^-} - C''_{Cl^-}}\right]} \tag{10}$$

for simple and shock waves, respectively. In these equations $\phi = (1 - \varepsilon)/\varepsilon$ is the phase ratio and

$$\frac{dq_{Cl^-}}{dC_{Cl^-}} = \frac{\partial q_{Cl^-}}{\partial C_{Cl^-}} + \frac{\partial q_{Cl^-}}{\partial C_{TRIS}} \frac{dC_{TRIS}}{dC_{Cl^-}} + \frac{\partial q_{Cl^-}}{\partial C_{HIS}} \frac{dC_{HIS}}{dC_{Cl^-}} + \frac{\partial q_{Cl^-}}{\partial C_{BTP}} \frac{dC_{BTP}}{dC_{Cl^-}} \tag{11}$$

Superscripts $'$ and $''$ represent values upstream and downstream of the shock front, respectively. In the earlier equations, q_{Cl^-} is given by the solution and ion exchange equilibrium relations, that is, Eqs. 2, 5, and 6.

The pH waves are determined by setting the characteristic or shock velocities equal for all components[27,38–40] and following the solution on the hodograph obtained by plotting the buffer concentration versus chloride concentration in a manner analogous to that shown in Ref. 31 for the case of a weak cation exchanger. Initial and final states in the column are represented by points on the hodograph and transitions from one state to the other are found on coherent paths connecting these states. When a buffer step is applied at the column entrance, the solution comprises a fast wave from the initial state, labeled I, to an intermediate state, labeled II, which corresponds to the passage of the unretained buffering species through the column. The fast wave is then followed by a slow wave from the intermediate state to the final state, labeled III, which corresponds to the exchange of Cl^- ions.[31] Because q_{Cl^-} does not change along the fast wave,[31] the chloride concentration of the intermediate state is found by setting

$$q^{I}_{Cl^-} = q^{II}_{Cl^-} \tag{12}$$

Thus, knowing the initial state ($C^{I}_{Cl^-}$, C^{I}_{TRIS}, C^{I}_{HIS}, C^{I}_{BTP}) and the final state ($C^{III}_{Cl^-} = C^{I}_{Cl^-}$, $C^{III}_{TRIS} = C^{II}_{TRIS}$, $C^{III}_{HIS} = C^{II}_{HIS}$, $C^{III}_{BTP} = C^{II}_{BTP}$), $C^{II}_{Cl^-}$ can be found by trial and error by determining the H^+ and Cl^- concentrations that simultaneously satisfy Eqs. 5 and 6.

After the intermediate state, the pH profile follows the path from II to III, along which C_{TRIS}, C_{HIS}, and C_{BTP} are constant. This path consists of either a plateau at II followed by a simple wave (with characteristic velocity described by Eqs. 9 and 11) if $v_{c_{Cl^-}}$ decreases from II to III or of a shock from II to III (with shock velocity described by Eq. 10) if $v_{c_{Cl^-}}$ increases from II to III. This path can also consist of shock followed by a gradual wave when $v_{c_{Cl^-}}$ initially increases and then decreases going from II to III. In this case, the chloride concentration where the wave transitions from shock to simple is determined by equating the shock and simple wave velocities. In each case, evaluation of the derivative $\partial q_{Cl^-}/\partial C_{Cl^-}$ is obtained numerically by taking small C_{Cl^-} increments.

Materials and Methods

Materials

The resins used in this study are DEAE Sepharose FF and ANX Sepharose 4 FF "high sub" (GE Healthcare, Piscataway, NJ). Both resins are based on similar agarose matrices and contain weak base groups. Table 1 summarizes the relevant properties. The extraparticle porosity, ε, and the intraparticle porosity, ε_p, of the columns packed with these resins were obtained as follows. For the DEAE resin, ε was obtained from pressure drop measurements in conjunction with the Carman–Kozeny equation. The value obtained for ε

Table 1. Summary of Sepharose FF Resin Properties

Property	DEAE	ANX
Particle size* (μm)	90	90
Extraparticle porosity, ε	0.30[†]	0.30[‡]
Intraparticle porosity, ε_p	0.80[§]	0.80[§]
Total base group content (μmol/mL)[¶]	110	160
n	4	1
pK_1	9.1	8.3
pK_2	8.2	–
pK_3	6.3	–
pK_4	5.4	–

*Manufacturer data. [†]Based on pressure drop measurements. [‡]Assumed to be the same as for DEAE Sepharose FF. [§]Based on retention of acetone. [¶]Values are per milliliters of packed column.

using this approach is comparable with those obtained for similar resins from the elution time of unretained macromolecular solutes that are excluded from the particle pores.[41] The same value of ε was thus assumed for the ANX resin, because the physical structure and particle sizes are the same for the two materials and the columns were packed with the same procedure. ε_p was obtained for both resins from the retention of an acetone pulse.

Buffer solutions were prepared with a fixed Cl^- concentration or with a fixed total concentration of buffering species. Solutions containing fixed Cl^- concentrations were prepared using ACS grade chemicals from Fisher Scientific (Fair Lawn, NJ) and Sigma Chemical Company (St. Louis, MO) by diluting standard 1 N HCl with distilled, deionized water and adding incremental amounts of the base component until the desired pH was reached. Mixed buffers containing the same Cl^- concentration and a desired ratio of buffering species were then prepared by mixing the single component buffer solutions in the appropriate proportions. Solutions with a fixed total concentration of buffering species were prepared by adding each free base to distilled, deionized water and titrating with concentrated HCl to the desired pH. After preparation, each buffer was degassed by vacuum filtering. It should be noted that the two types of buffer preparations are not equivalent and result in different column behavior. For example, a buffer solution containing 0.01 M TRIS at pH 7 will contain less than 0.01 M Cl^-. In turn, because protein binding in ion exchange depends principally on the concentration of the counterion,[42–44] protein retention will be stronger than in a TRIS buffer containing 0.01 M Cl^- at the same pH.

Bovine apo-transferrin was obtained from Sigma Chemical (St. Louis, MO). Transferrin is a globular protein with an approximate molecular mass of 78,000 Da and a pI around 6.[32] The protein is known to contain different sialytated charge variants.[32,45,46] A monoclonal antibody (mAb) was provided by Pfizer (St. Louis, MO). As demonstrated by IEF analyses, the mAb sample comprises several charge variants. In both cases, protein solutions were prepared in 1–5 mg/mL concentrations.

Potentiometric titrations

Potentiometric titrations of the resins were conducted as follows. A sample of each resin (2 mL) was flow packed in 0.5 × 10 cm Tricorn column (GE Healthcare, Piscataway, NJ) at 2 mL/min and equilibrated with 0.1 M NaCl adjusted to pH 11 with NaOH. The packed resin was then manually extruded from the column into 25–50 mL of 0.1 M NaCl at pH 11, and titrated with standardized 0.01 M HCl while monitoring the pH. Theoretical and experimental titration curves can then be related by considering the following equations:

$$C_{Na^+} + C_{H^+} = C_{Cl^-} + C_{OH^-} = C_{Cl^-} + K_w/C_{H^+} \quad (13)$$

$$m_{HCl} = C_{Cl^-}V + \left(q_{Cl^-} - q^0_{Cl^-}\right)V_R - C^0_{Cl^-}V_0 \quad (14)$$

where m_{HCl} is the moles of HCl added, V and V_0 are the current and initial volumes of solution, $q^0_{Cl^-}$ and $C^0_{Cl^-}$ are the initial resin and solution phase concentrations, respectively, and V_R is the resin volume. q_{Cl^-} is related to the solution pH and Cl^- concentration through Eqs. 5 and 6. Thus, the volume of titrant HCL added at each pH can be determined by solving the Eqs. 5, 6, 13, and 14 simultaneously. The total concentration of weak acid groups, q_0, and the resins' pK-values were then determined by fitting the titration curves predicted from these equations to the experimentally determined ones.

Column pH transients

Column experiments were conducted with an ÄKTA Explorer system (GE Healthcare, Piscataway, NJ) with the resins packed in either 0.5 × 20 cm Tricorn columns (GE Healthcare) or in 1.1 × 20 cm Vantage-L columns (Millipore, Billerica, MA). pH gradients were generated by implementing step changes in buffer composition after loading the protein with the system load pump. Effluent conductivity and pH were monitored with the ÄKTA system instrumentation although fractions were also collected and tested offline with a calibrated meter (Model S20 Mettler-Toledo, Columbus, OH). Conductivity traces were converted to chloride concentration for a qualitative comparison with the model predictions by assuming a linear relationship with Cl^- concentration.

Analytical IEF

IEF analyses were conducted on samples of the crude protein and on selected fractions from the pH gradient runs. For apo-transferrin IEF was conducted using Novex pH 3–7 precast vertical mini gels and buffers obtained from Invitrogen (Carlsbad, CA) with 0.75–1.5 μg protein loads. Following electrophoresis, the gel was fixed with a solution containing 12% trichloroacetic acid and 3.5% sulfosalicylic acid for 30 min. Protein bands were visualized using Colloidal Coomassie Blue G-250 stain from Invitrogen. Gel images were recorded using a Bio-Rad (Hercules, CA) GS-800 calibrated densitometer.

IEF analysis of mAb samples was conducted in a similar way but using IsoGel pH 7–11 agarose plates obtained from Lonza (Walkersville, MD) with 2–4 μg protein loads.

Results and Discussion

Resin titrations

The experimental titration curves are shown in Figure 1. Starting at high pH, the amount of HCl added increases gradually at first and then reaches a plateau corresponding to the resin's total concentration of weak acid groups. At pH values lower than this point, the titration curves rise sharply because the resin has lost all its buffering capacity.

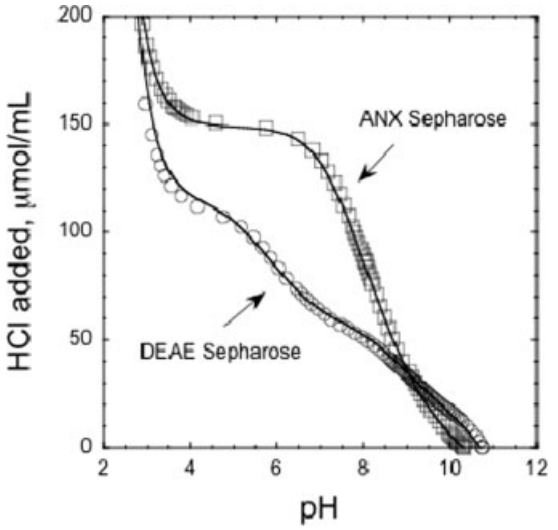

Figure 1. Potentiometric titration curves for DEAE Sepharose FF and ANX Sepharose FF resins.

Lines are calculated from Eqs. 5, 6, 13, and 14. Experimental conditions are noted in text and model parameters are given in Table 1.

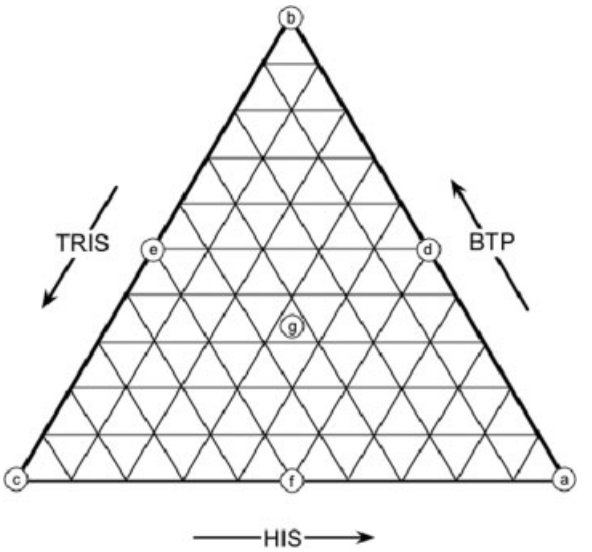

Figure 2. Ternary diagram showing buffer compositions with 0.02 M Cl^- used to generate pH 7–5 gradients with DEAE Sepharose.

The corresponding experimental results and model predictions are shown in Figure 3.

Calculated titration curves obtained from Eqs. 5, 6, 13, and 14 based on the fitted parameters given in Table 1 are also shown. As seen in Figure 1, in the case of ANX Sepharose, a satisfactory fit of the data could be obtained with a single pK value ($n = 1$). Conversely, four different pK-values ($n = 4$) were needed to accurately describe the DEAE Sepharose data. Although the exact reasons for this difference are not known, the results are consistent with information from the resin manufacturer that ANX contains exclusively truly weak base groups and is thus more chemically homogeneous than the DEAE resin.[47]

Induced pH gradients

Implementing separations based on internally produced pH gradients is dependent on the ability to predict the buffer compositions that will generate gradients of appropriate slope. Thus a broad range of buffer compositions was tested experimentally with DEAE Sepharose and the results compared with model predictions. The buffer compositions tested for pH 7–5 steps are represented in Figure 2 for TRIS, BTP, HIS, and their mixtures, all with a 0.02 M chloride concentration. The experimental pH profiles obtained for each condition indicated are shown in Figure 3 along with those predicted by the local equilibrium model.

In all cases, a fast wave emerges from the column in about 1 CV, which corresponds to the passage of the unretained buffer species. The ensuing plateau has chloride concentration and pH that are lower than those of the initial buffer. Their values are dependent on the buffer employed. For example, HIS, whose pK_a is closest to the step pH, results in a large decrease in chloride concentration and pH at the intermediate state. On the other hand, TRIS, whose pK_a is farthest from the step pH, results in only a small decrease in chloride concentration and pH at the intermediate plateau. The BTP buffer and mixtures of the three buffers fall in between the two extremes. As discussed in "Column dynamics" section, a slow wave follows the initial plateau and has a shape that is dependent on the particular buffer employed. Using HIS only (point a in Figure 2) or buffer mixtures containing HIS (points d, f, and g in Figure 2), the pH profiles consist of a shock transition followed by a gradual wave. This combined wave behavior occurs because, in these cases, the chloride binding isotherm, plotted with constant buffer concentration, has an inflection point, transitioning from a favorable shape (i.e. concave downward) to an unfavorable one (i.e. concave upward) as the Cl^- concentration increases from the intermediate plateau value to the final value. As a result, we obtain a shock for the favorable portion, followed by a gradual wave. The chloride concentration where the wave transitions from shock to gradual is found by equating shock and simple wave velocities according to the so-called "Golden rule."[48]

On the other hand, for TRIS, BTP, and their mixtures (points b, c in Figure 2) the pH profile following the initial plateau is just a gradual wave. This occurs because in these cases the chloride binding isotherm remains unfavorable (i.e. concave upward) as the Cl^- concentration increases from the intermediate plateau value to the final value. However, compared with BTP, TRIS results in extremely shallow gradients. For example, using TRIS alone (point c in Figure 2) results in a gradient that reaches the final pH of 5 in 608 CV. Such a long gradient may result in substantial resolution, but is probably impractical. BTP, on the other hand, provides fairly shallow smooth gradients that are not excessively long. For example, BTP alone (point b in Figure 2) reaches pH 5 in 101 CV.

In all cases, the agreement between experimental and predicted curves is excellent. Because parameters determined from the titration curve were used in the model calculations without adjustment, the lines shown are true predictions. Significant deviations are seen only when shocks are formed. This is because the model assumes local equilibrium and plug flow with no axial dispersion. In practice, however, some flow non-idealities obviously exist in these columns (e.g. see Ref. 49) resulting in experimental profiles that are smoother than the shock transitions predicted.

As is obvious from these results, in practice, shallow gradients can be obtained using a simple single component

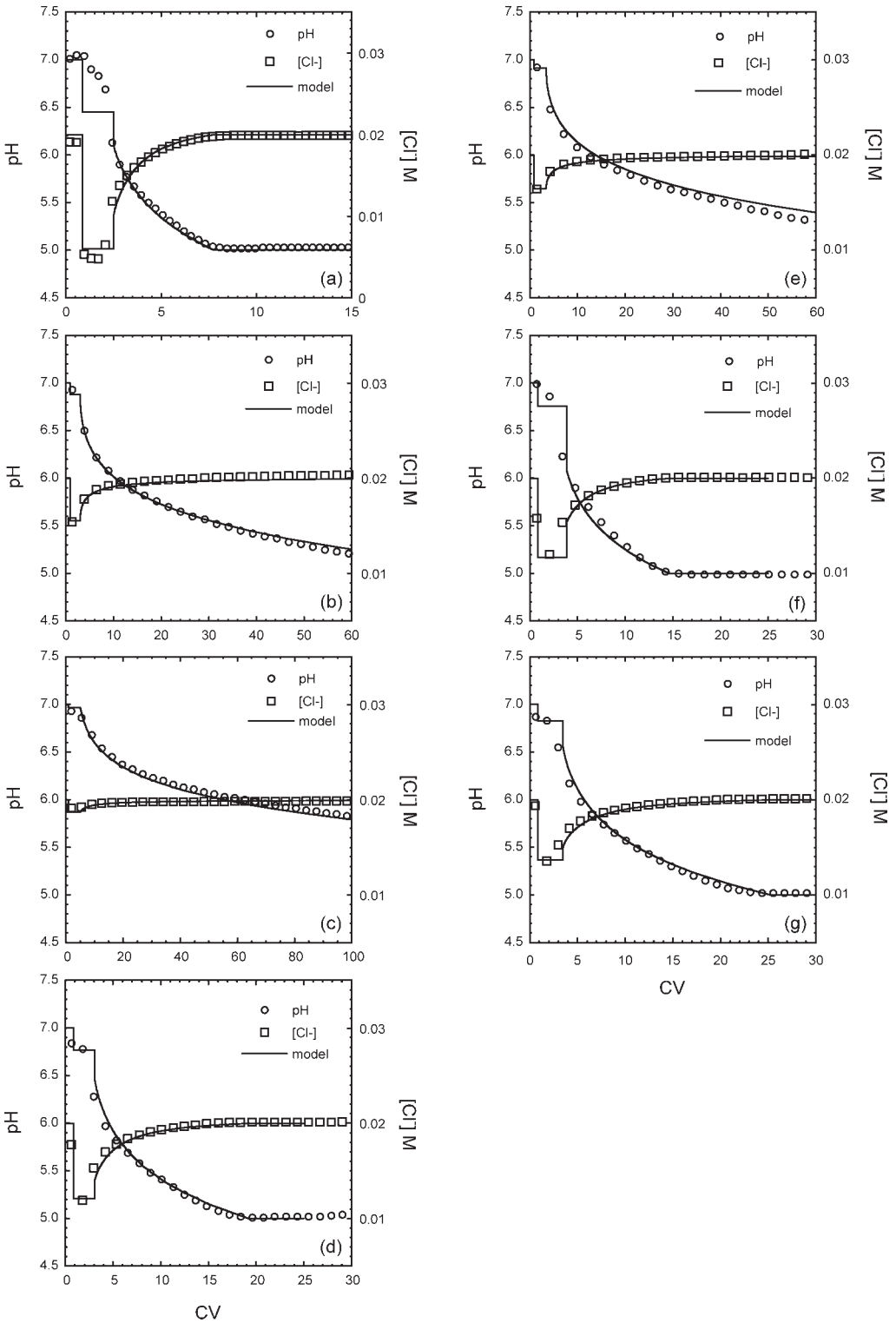

Figure 3. Experimental and predicted Cl^- concentration profiles and pH transitions for pH 7–5 steps in a 0.5 × 20 cm DEAE Sepharose column at 1 mL/min with buffers containing 0.02 M Cl^- for the following buffers.

(a) HIS, (b) BTP, (c) TRIS, (d) equimolar HIS/BTP, (e) equimolar BTP/TRIS, (f) equimolar HIS/TRIS, (g) equimolar HIS/BTP/TRIS. Lines are based on the local equilibrium model with parameters in Table 1.

buffer system provided the buffer pK_a is approximately 2 pH unit above the operating pH. This rule of thumb will vary from resin to resin, and with buffer concentration, but it is a good place to start when designing shallow pH gradients.

Two additional effects of the buffer composition are shown in Figure 4 for buffers containing only BTP. Figure 4a shows the effect of chloride concentration (and hence buffer concentration) on the pH profiles generated by pH 7–5 buffer steps with DEAE Sepharose, whereas Figure 4b shows the effect of using buffer steps with different initial and final pH values. As seen in Figure 4a, decreasing the buffer Cl^- concentration prolongs the length of the induced pH gradient. Conversely, as seen in Figure 4b varying the initial and final pH values affect only the plateau region of the profile. The

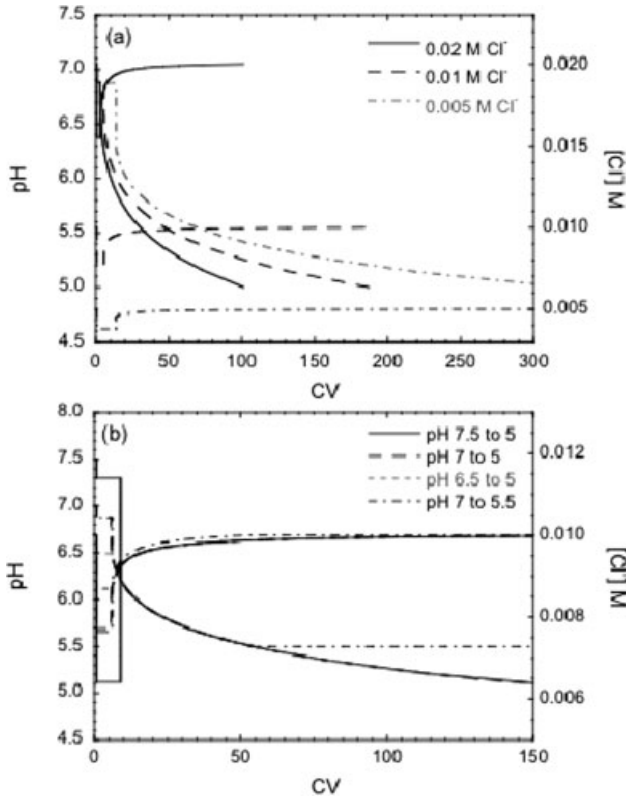

Figure 4. Predicted pH transitions for BTP buffer steps with DEAE Sepharose.

(a) Effect of Cl^- concentration for pH 7–5 BTP buffer steps; (b) Effect of initial and final pH for BTP buffer steps with 0.01 M Cl^-.

gradual wave that follows has the same shape and duration until the final pH is attained.

As a final example, Figure 5 shows a comparison of the predicted pH and Cl^- profiles for DEAE and ANX Sepharose generated with pH 9.5–8 steps using 0.01 M ethanolamine as the buffer. Experimental pH profiles are also shown. Gradual waves are obtained in both cases. However, the ANX profile is much shallower because, as seen in Figure 1, this resin has a substantially greater buffering capacity over this range of pH values. Model predictions are again in good agreement with the experimental results.

Separation of apo-transferrin charge variants

The resolution of apo-transferrin charge variants was obtained with pH gradients from 7 to 5 generated by buffer steps with 0.01 M Cl^- concentrations using a DEAE Sepharose column. Figure 6 shows a representative result obtained with BTP buffers at 1 mL/min (300 cm/h). Although the resolution is obviously limited, IEF analyses of fractions collected at the points indicated by the arrows show a substantial separation of the protein charge variants along the induced pH gradient. Although fractions 1 and 2 contain three and two variants, respectively, of the five major variants present in the protein sample, fractions 3 and 4 contain only one major variant. As confirmed by IEF, the variants elute in order of decreasing isoelectric point. When the pH step occurs at the top of the column, each variant instantly becomes trapped along a pH wave where its chromatographic velocity is equal to that of the pH wave. More acidic

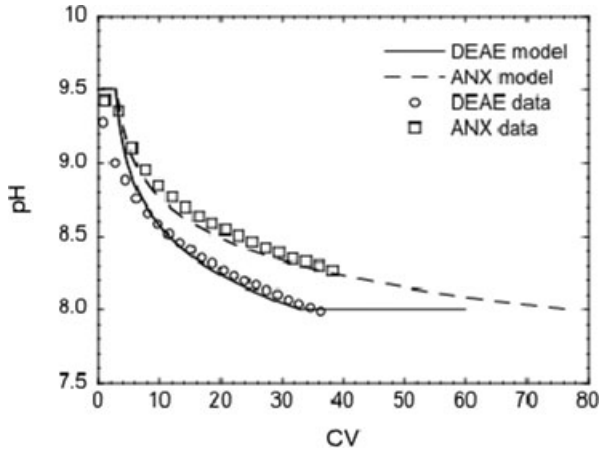

Figure 5. Experimental and predicted pH profiles for DEAE and ANX Sepharose generated with pH 9.5–8 steps using 0.01 M ethanolamine in 1.1 × 20 cm columns at 1.6 mL/min (100 cm/h).

Lines are based on the local equilibrium model with parameters in Table 1.

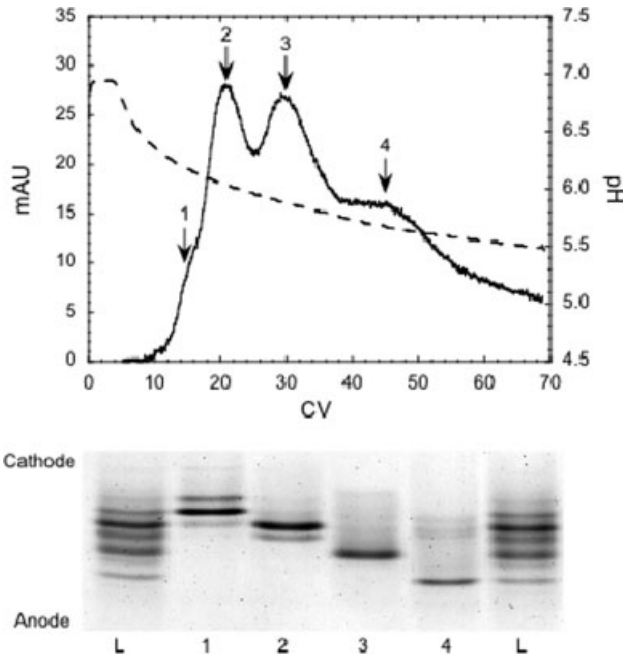

Figure 6. Chromatographic separation of apo-transferrin charge variants using a pH 7 to 5 BTP buffer step with 0.01 M Cl^- in a 0.5 × 20 cm DEAE Sepharose column at 1 and 5 mg/mL protein load.

Dashed line shows the experimental induced pH gradient. Bottom graph shows IEF analyses of peak fractions indicated. Lanes labeled "L" are the crude protein load.

species accumulate closer to the anode in the IEF gel and are retained longer in the column.

Various conditions were explored to determine their effects on resolution. Figure 7 shows the effects of the buffer type on the separation of apo-transferrin charge variants using pH 7–5 steps with equal 0.02 M Cl^- concentrations. As seen in Figure 7, the conductivity remains low and nearly constant when the protein elutes. Thus separation is primarily determined by the induced pH gradient shape and length. In the case of HIS (Figure 7a) the induced pH gradient is steep (8 CV) and there is no discernible resolution of charge

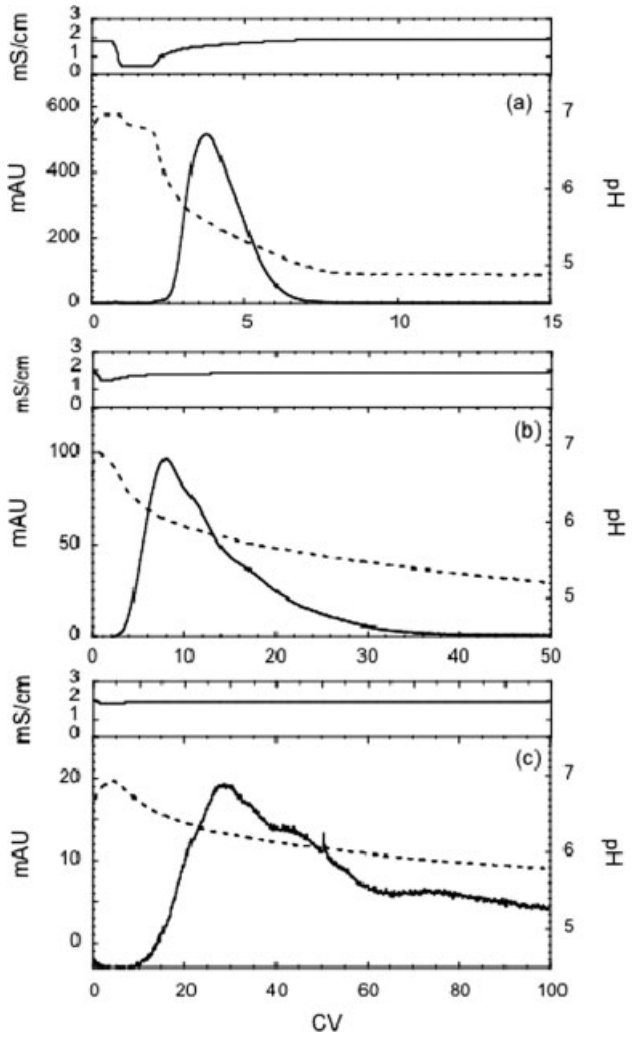

Figure 7. Effect of buffer type on the chromatographic separation of apo-transferrin charge variants using pH 7–5 BTP buffer steps with 0.02 M Cl^- in a 0.5 × 20 cm DEAE Sepharose column at 1 mL/min.

Protein load was 5 mg/mL. Upper traces show the conductivity profiles. (a) HIS, (b) BTP, (c) TRIS.

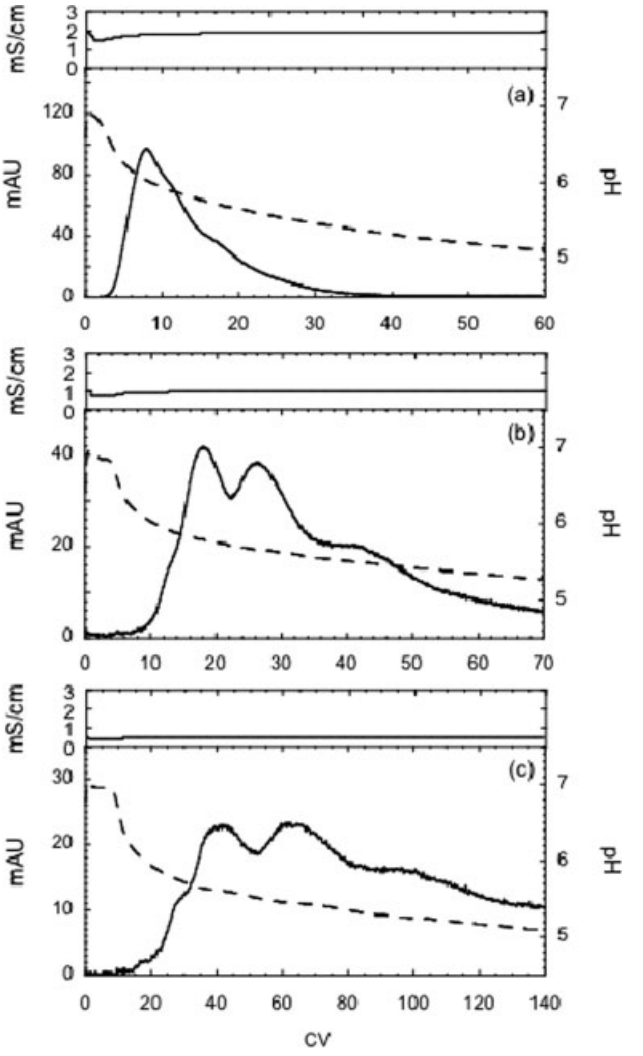

Figure 8. Effect of Cl^- concentration on the chromatographic separation of apo-transferrin charge variants using pH 7–5 BTP buffer step in a 0.5 × 20 cm DEAE Sepharose column at 1 and 5 mg/mL protein load and 1 mL/min.

Dashed line shows the induced pH gradient. (a) 0.02 M Cl^-, (b) 0.01 M Cl^-, (c) 0.005 M Cl^-.

variants. Some resolution is evident using BTP (Figure 7b), although, for these conditions elution occurs in the first 20 CV, where the pH gradient is steep so that resolution is again limited. Better resolution is obviously evident for TRIS (Figure 7c), which results in a shallow gradient.

Figure 8 shows the effect of the buffer chloride concentration (and thus buffer concentration) for pH 7–5 gradients generated using BTP with the DEAE Sepharose column at 1 mL/min. Protein was loaded to 5 mg/mL of packed bed. The effect is complex because the chloride concentration affects the pH profile, as previously shown, as well as the protein retention. Longer pH gradients are formed with lower chloride concentrations, which lead to higher resolution of variants. Increasing ionic strength leads to weaker binding, and less protein retention. Thus, the charge variants elute earlier in the induced gradient at higher pH-values. For the results shown in Figure 8, the apo-transferrin variants elute in the pH range of 5.75–6.1 for 0.02 M Cl^-, 5.5–5.75 for 0.01 M, and 5.2–5.7 for 0.005 M.

Figure 9 shows the effect of the initial pH for pH gradients generated using BTP buffer steps to pH 5 with equal 0.01 M Cl^- concentrations. pH gradients that started at pH 7.5, 7, and 6.5 all had shock transitions to pH 6.4, followed by identical gradual waves, a result consistent with prediction based on the local equilibrium model. As seen in Figure 9, a consequence of this result is that the effect of the initial pH on resolution is limited.

Figure 10 shows the effect of flow rate with 5 mg/mL protein load. Conductivity and pH traces show very little sensitivity to the flow rate confirming that the ion exchange processes involved in generating the induced gradient are not mass transfer limited. Remarkably, the resolution also shows relatively little sensitivity to flow despite the fact that the superficial velocity is increased by a factor of 4 and that the particles are 90 μm in size. As discussed in Pabst et al.,[31] this occurs because of the axial pH gradient established in the column as a result of the interaction of the mobile phase components with the resin. These authors showed that proteins separated with internally generated pH gradients had HETP values nearly 10-fold lower than expected based on the generalized HETP expression of Snyder and Kirkland.[50]

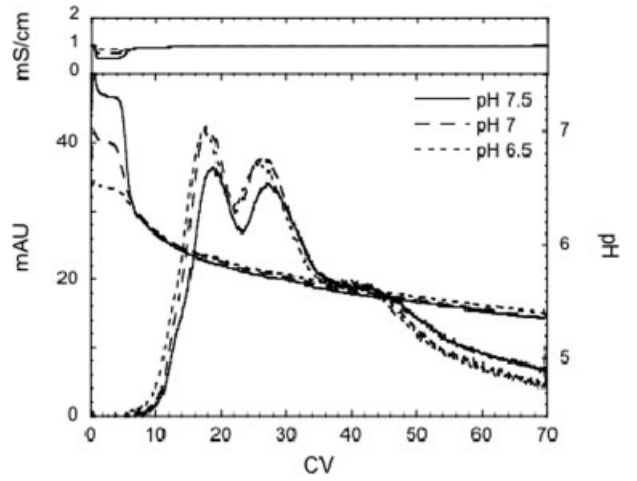

Figure 9. Effect of initial pH on the chromatographic separation of apo- transferrin charge variants using BTP buffer steps with 0.01 M Cl^- in a 0.5 × 20 cm DEAE-Sepharose column.

Protein load was 5 mg/mL. Upper traces show the conductivity profiles. The final pH was 5 in all cases.

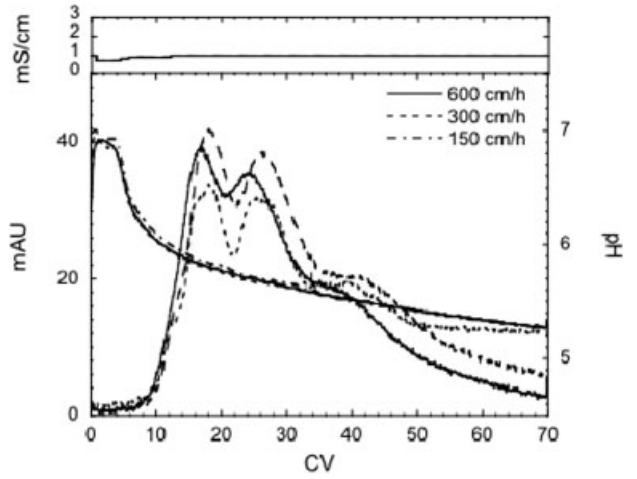

Figure 10. Effect of flow rate on the chromatographic separation of apo-transferrin charge variants using pH 7–5 BTP buffer steps with 0.01 M Cl^- in a 0.5 × 20 cm DEAE Sepharose column.

Protein load was 5 mg/mL. Upper traces show the conductivity profiles.

Therefore when the increased flow rate does broaden the peak, the axial pH gradient tends to compress it. Thus, sharper bands and greater resolution are obtained with the induced pH gradients,

Separation of mAb charge variants

Figures 11 and 12 show the resolution of mAb charge variants obtained using pH 9.5–8 steps with 0.01 M ethanolamine buffers at 100 cm/h for DEAE Sepharose and ANX Sepharose columns, respectively. The mAb contains three major charge variants, which were fully resolved by imaging capillary electrophoresis—iCE (results not shown). As seen from the accompanying IEF analyses in Figures 11 and 12, two of these variants appear as a single broader band, whereas the third is fully resolved. Remarkably, however, while the separation is not complete all three major variants

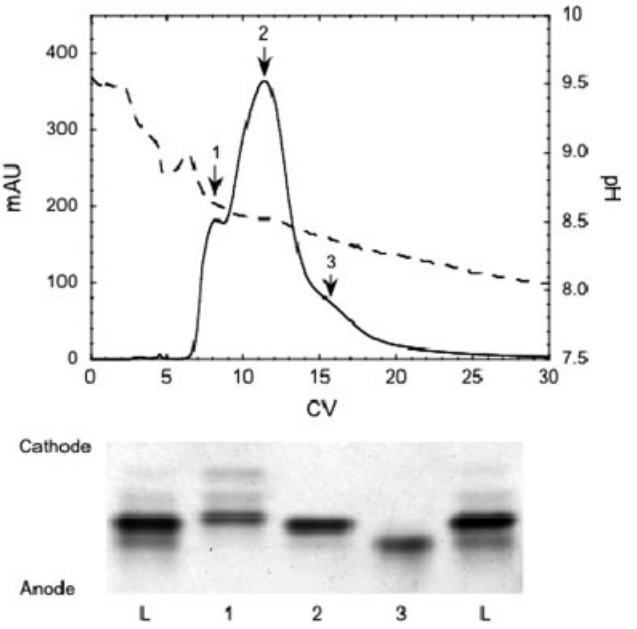

Figure 11. Chromatographic separation of mAb charge variants using a pH 9.5–8 buffer step with 0.01 M ethanolamine in a 1.1 × 20 cm DEAE Sepharose column at 1.6 mL/min (100 cm/h) and 5 mg/mL protein load.

Dashed line shows the experimental induced pH gradient. Bottom graph shows IEF analyses of peak fractions indicated. Lanes labeled "L" are the crude protein load.

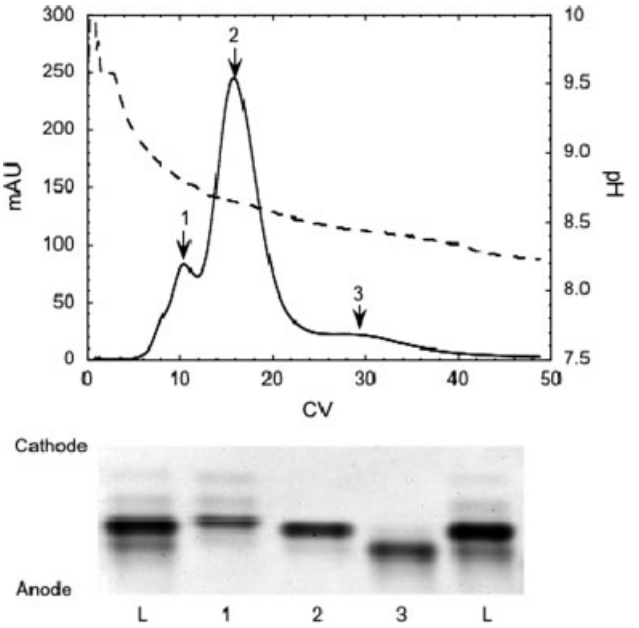

Figure 12. Chromatographic separation of mAb charge variants using a pH 9.5–8 buffer step with 0.01 M ethanolamine in a 1.1 × 20 cm ANX Sepharose column at 1.6 mL/min (100 cm/h) and 5 mg/mL protein load.

Dashed line shows the experimental induced pH gradient. Bottom graph shows IEF analyses of peak fractions indicated. Lanes labeled "L" are the crude protein load.

are resolved in fractions collected at the apexes of the peaks obtained in both columns with the induced pH gradients. The resolution is better with the ANX Sepharose and this result is likely due to the shallower gradient that, as

discussed previously, is generated for this particular pH range. In both cases, however, the order of elution of the variants follows the order of their pIs as determined by IEF.

Conclusions

The local equilibrium model developed in this work provides accurate quantitative predictions of the pH gradients induced by step changes in buffer composition with weak base anion exchange columns. The model predictions, based only on the resin's potentiometric titration, are validated over a broad range of buffer types, ionic strength, initial and final pH, and flow rate. Application of the induced pH gradients to the separation of charge variants provided remarkable results. As confirmed by IEF analyses, the induced pH gradients provide charge variant resolution at low ionic strengths, with large particle sizes, high flow rates, and substantial protein loads. Thus, the technique appears suitable to solve the difficult industrial separation problems that arise when charge variants, which are sometimes present in therapeutic protein products, need to be separated. One aspect that will require further study is the effect of protein load. The loads used in this work are higher than previously used in chromatofocusing studies and are considerable for high-resolution applications. On the other hand, the absolute limits are currently not known and will be explored in future work.

Acknowledgments

This research was supported by Pfizer and the NIH Biotechnology Training program at the University of Virginia. The authors thank Pfizer Process Development Analytical group for assistance with IEF and iCE analysis of mAb samples.

Notation

C = liquid phase concentration
CV = number of column volumes ($=\varepsilon vt/L$)
K = resin phase dissociation constant
K_a = buffer dissociation constant
K_w = ionic product of water
L = column length
q = resin phase concentration
$\bar{q}$ = concentration averaged over particle volume
t = time
v = mobile phase velocity
V = solution volume
V_0 = initial value of V
V_R = resin volume
z = column axial coordinate
ε = extraparticle void fraction
ε_p = intraparticle void fraction
ϕ = phase ratio [$=(1-\varepsilon)/\varepsilon$]
γ_i = activity coefficient

Literature Cited

1. Kroon DJ, Freedy J, Burinsky DJ, Sharma B. Rapid profiling of carbohydrate glycoforms in monoclonal antibodies using MALDI/TOF mass spectrometry. *J Pharm Biomed Anal*. 1995; 13:1049–1054.
2. Covalt JC Jr, Cao TB, Magdaroag JRC, Jennings PA, Gross LA. Temperature, media, and point of induction affect the N-terminal processing of interleukin-1β. *Protein Exp Purif*. 2005; 41:45–52.
3. Werner RG, Kopp K, Schlueter M. Glycosylation of therapeutic proteins in different production systems. *Acta Paediatr*. 2007; 96:17–22.
4. Sharma B. Immunogenicity of therapeutic proteins, Part 3: Impact of manufacturing changes. *Biotechnol Adv*. 2007;25: 325–331.
5. Yem AW, Richard KA, Staite ND, Deibel MR, Jr. Resolution and biological properties of three N-terminal analogues of recombinant human interleuken-1β. *Lymphokine Res*. 1988;7: 85–92.
6. Harris RJ, Kabakoff B, Macchi FD, Shen FJ, Kwong M, Andya JD, Shire SJ, Bjork N, Totpal K, Chen AB. Identification of multiple sources of charge heterogeneity in a recombinant antibody. *J Chromatogr B*. 2001;752:233–245.
7. Scallon BJ, Tam SH, McCarthy SG, Cai AN, Raju TS. Higher levels of sialylated Fc glycans in immunoglobulin G molecules can adversely impact functionality. *Mol Immunol*. 2007;44: 1524–1534.
8. Fukuda MN, Sasaki H, Lopez L, Fukuda M. Survival of recombinant erythropoietin in the circulation: The role of carbohydrates. *Blood*. 1989;73:84–89.
9. Sinclair, AM, Elliott, S. Glycoengineering: The effect of glycosylation on the properties of therapeutic proteins. *J Pharm Sci*. 2005;94:1626–1635.
10. D'Antonio M, Borrelli F, Datola A, Bucci R, Mascia M, Polletta P, Piscitelli D, Papoian R. Biological characterization of recombinant human follicle stimulating hormone isoforms. *Hum Reprod*. 1999;14:1160–1167.
11. Creus S, Chaia Z, Pellizzari EH, Cigorraga SB, Ulloa-Aguirre A, Campo S. Human FSH isoforms: Carbohydrate complexity as determinant of in-vitro bioactivity. *Mol Cell Endocrinol*. 2001;174:41–49.
12. Elliott S, Lorenzini T, Asher S, Aoki K, Brankow D, Buck L, Busse L, Chang D, Fuller J, Grant J, Hernday N, Hokum M, Hu S, Knudten A, Levin N, Komorowski R, Martin F, Navarro R, Osslund T, Rogers G, Rogers N, Trail G, Ergie J. Enhancement of therapeutic protein in vivo activities through glycoengineering. *Nat Biotechnol*. 2003;21:414–421.
13. Perlman S, van den Hazel B, Christiansen J, Gram-Nielsen S, Jeppesen CB, Andersen KV, Halkier T, Okkels S, Schambye HT. Glycosylation of an N-terminal extension prolongs the half-life and increases the in vivo activity of follicle stimulating hormone. *J Clin Endocrinol Metab*. 2003;88:3227–3235.
14. Weitzhandler M, Farnan D, Horvath J, Rohrer JS, Slingsby RW, Avdalovic N, Pohl C. Protein variant separations by cation-exchange chromatography on tentacle-type polymeric stationary phases. *J Chromatogr A*. 1998;828:365–372.
15. Yamamoto S, Ishihara T. Ion-exchange chromatography of proteins near the isoelectric point. *J Chromatogr A*. 1999;852:31–36.
16. de la Calle Guntiñas MB, Bordin G, Rodriguez AR. Study of the feasibility of using a pellicular anion-exchange column for separation of transferrin isoforms in human serum by HPLC with UV detection. *Anal Bioanal Chem*. 2004;378:383–387.
17. Perkins M, Theiler R, Lunte S, Jeschke M. Determination of the origin of charge heterogeneity in a murine monoclonal antibody. *Pharm Res*. 2000;17:1110–1117
18. Monkarsh SP, Russoman EA, Roy SK. Separation of interleukins by a preparative chromatofocusing-like method. *J Chromatogr*. 1993;631:277–280.
19. Mhatre R, Nashabeh W, Schmalzing D, Yao X, Fuchs M, Whitney D, Regnier F. Purification of antibody Fab fragments by cation-exchange chromatography and pH gradient elution. *J Chromatogr A*. 1995;707:225–231.
20. Ahamed T, Nfor BK, Verhaert PDEM, van Dedem GWK, van der Wielen LAM, Eppink MHM, van de Sandt EJAX, Ottens M. pH-gradient ion-exchange chromatography: An analytical tool for design and optimization of protein separations. *J Chromatogr A*. 2007;1164:181–188.
21. Sluyterman LAAE, Elgersma O. Chromatofocusing: Isoeletric focusing on ion-exchange columns. I. General principles. *J Chromatogr*. 1978;150:17–30.

22. Sluyterman LAAE, Wijdenes J. Chromatofocusing: Isoeletric focusing on ion-exchange columns. II. Experimental verification. *J Chromatogr*. 1978;150:31–44.
23. Strong JC, Frey DD. Experimental and numerical studies of the chromatofocusing of dilute proteins using retained pH gradients formed on a strong-base anion-exchange column. *J Chromatogr A*. 1997;769:129–143.
24. Scott JH, Kelner KL, Pollard HB. Purification of synexin by pH step elution from chromatofocusing media in the absence of ampholytes. *Anal Biochem*. 1985;149:163–165.
25. Logan KA, Lagerlund I, Chamow SM. A simple, two-component buffer enhances use of chromatofocusing for processing of therapeutic proteins. *Biotechnol Bioeng*. 1999;62:208–215.
26. Bates RC, Kang X, Frey DD. High-performance chromatofocusing using linear and concave pH gradients formed with simple buffer mixturesIEffect of buffer composition on the gradient shape. *J Chromatogr A*. 2000;890:25–36.
27. Kang X, Bates RC, Frey DD. High-performance chromatofocusing using linear and concave pH gradients formed with simple buffer mixturesIISeparation of proteins. *J Chromatogr A*. 2000;890:37–43.
28. Kang X, Frey DD. High-performance cation-exchange chromatofocusing of proteins. *J Chromatogr A*. 2003;991:117–128.
29. Pabst TM, Carta G. pH transitions in cation exchange chromatographic columns containing weak acid groups. *J Chromatogr A*. 2007;1142:19–31.
30. Bates RC, Frey DD. Quasi-linear pH gradients for chromatofocusing using simple buffer mixtures: Local equilibrium theory and experimental verification. *J Chromatogr A*. 1998; 814:43–54.
31. Pabst TM, Antos D, Ramasubramanyan N, Hunter A, Carta G. Protein separations with induced pH gradients using cation exchange chromatographic columns containing weak acid groups. *J Chromatogr A*. 2008;1181:83–94.
32. Yang L, Tang Q, Harrata AK, Lee CS. Capillary isoelectric focusing–electrospray ionization mass spectrometry for transferrin glycoforms analysis. *Anal Biochem*. 1996;243:140–149.
33. Beynon RJ, Easterby JS. *Buffer Solutions—The Basics*. Oxford: Oxford University Press; 1996:69.
34. Lide DR, editor. *CRC Handbook of Chemistry and Physics*, 88th Edition (Internet Version 2008), Section 7. Boca Raton, FL: CRC Press/Taylor and Francis; 2008.
35. Davies CW. *Ion Association*. London: Butterworths; 1962:37–48.
36. Stoyanov AV, Righetti PG. Dissociation of polyvalent electrolytes. *J Chromatogr A*. 1999;853:35–44.
37. Helfferich F. *Ion Exchange*. New York: McGraw-Hill; 1962: Section 4:72–94.
38. Helfferich F, Klein G. *Multicomponent Chromatography: Theory of Interference*. Ann Arbor: Marcel Dekker; 1970.
39. Ruthven DM. *Principles of Adsorption and Adsorption Processes*. New York: Wiley; 1984.
40. Soto Pérez J, Frey DD. Behavior of the inadvertent pH transient formed by a salt gradient in the ion-exchange chromatography of proteins. *Biotechnol Progr*. 2005;21:902–910.
41. De Phillips P, Lenhoff AM. Pore size distributions of cation-exchange adsorbents determined by inverse size-exclusion chromatography. *J Chromatogr A*. 2000;883:39–54.
42. Rounds MA, Regnier FE. Evaluation of a retention model for high-performance ion-exchange chromatography using two different displacing salts. *J Chromatogr*. 1984;283:37–45.
43. Yamamoto S, Nakanishi K, Matsuno R. *Ion Exchange Chromatography of Proteins*. New York: Marcel Dekker; 1988.
44. Brooks CA, Cramer SM. Steric mass-action ion exchange: Displacement profiles and induced salt gradients. *AIChE J*. 1992; 38:1969–1978.
45. Stratil A, Spooner, RL. Isolation and properties of individual components of cattle transferrin: The role of sialic acid. *Biochem Genet*. 1971;5:347–365.
46. Richardson NE, Buttress N, Feinstein A, Stratil A, Spooner RL. Structural Studies on individual components of bovine transferrin. *Biochem J*. 1973;135:87–92.
47. ANXSepharose 4 Fast Flow (high sub). Amersham Biosciences Data File, GE Healthcare, Piscataway, NJ, 2000.
48. Frey DD. The entropy condition for the dynamics of nonlinear multicomponent sorption in porous media. *Chem Eng Sci*. 1990; 45:131–142.
49. Farkas T, Sepaniak MJ, Guiochon G. Radial distribution of the flow velocity, efficiency and concentration in a wide HPLC column. *AIChE J*. 1997;43:1964–1974.
50. Snyder LR, Kirkland JJ. *Introduction to Modern Liquid Chromatography*, 2nd ed. New York: Wiley; 1979:234–240.

Manuscript received Nov. 9, 2007, and revision received Feb. 18, 2008.

BTPR070432E